Desalination and Water Treatment
www.deswater.com

doi:10.5004/dwt.2017.20421

73 (2017) 380–388
April

Removal of tetracycline by magnetic chitosan nanoparticles from medical wastewaters

Parinaz Raeiatbin[a], Yeşim Sağ Açıkel[b,*]

[a]*Hacettepe University, Bioengineering Division, Institute of Science, 06800, Beytepe, Ankara, Turkey, email: parinaz@hacettepe.edu.tr*
[b]*Hacettepe University, Chemical Engineering Department, 06800, Beytepe, Ankara, Turkey, Tel. +90 312 297 74 44, Fax +90 312 299 21 29, email: yesims@hacettepe.edu.tr*

Received 23 June 2016; Accepted 10 December 2016

ABSTRACT

In this study, chitosan (CHT)-based nanoparticles loaded with iron oxide (Fe_3O_4) nanoparticles were gained magnetic properties. The coating of CHT onto the iron oxide nanoparticles was confirmed by Fourier transform infrared (FTIR) spectroscopy, thermogravimetric analysis (TGA) and differential scanning calorimetry analysis (DSC). The effects of the initial pH value of tetracycline solution, the amount of CHT-Fe_3O_4 nanoparticles, the initial concentration of tetracycline solution on the removal of tetracycline by CHT MNPs were investigated in batch reactors operated at 25°C. The maximum amount of adsorbed tetracycline per unit weight of CHT MNPs at equilibrium and adsorption efficiency obtained at 50 mg/L initial tetracycline concentration, at pH 5.0 and at 0.5 g/L CHT MNPs concentration was found to be 78.11 mg/g and 78.8 %, respectively. The equilibrium adsorption of tetracycline by CHT MNPs was represented by the Langmuir and Freundlich adsorption models. The adsorption kinetics of tetracycline on CHT MNPs was represented better by the pseudo-second-order rate equation than by Lagergren pseudo-first order rate equation.

Keywords: Medical wastewaters; Tetracycline; Magnetic chitosan nanoparticles (CHT MNPs); Adsorption

1. Introduction

Tetracyclines ($C_{22}H_{24}N_2O_8$) are the second most widely used antibiotics in the world to prevent and treat a range of infectious diseases due to broad-spectrum antibacterial activity in human and veterinary medicine. Chlortetracycline and oxytetracycline are commonly used in animal feed as growth promoters and prophylactics. Significant fractions of pharmaceutically active compounds are excreted in their unmetabolised form and their residues left in the environment, which are potentially toxic to aquatic organisms and human health through the food chain and drinking water. These bioactive compounds accumulated in the soil, surface water and ground water may promote the development and spread of antibiotic resistant genes among bacterial populations or induce biological responses in nontarget organisms due to prolonged exposures to low-level antibiotics [1,2]. Consequently, the removal of tetracyclines from waste waters is of great significance. Ozonation, photo-Fenton process, photoelectrocatalytic degredation, and adsorption have been used for the removal of tetracycline from water. Among these methods, adsorption is considered as one of the most effective techniques, due to simple reactor design, easy operation conditions, high treatment efficiency, and low cost [3–6].

The use of adsorbents composed of natural polymers obtained from algal or fungal cells and shellfish has attracted significant interest, and polysaccharides such as chitin and chitosan and its derivatives have received particular attention [7]. Chitin is a linear homopolymer

*Corresponding author.

Presented at the EDS conference on Desalination for the Environment: Clean Water and Energy, Rome, Italy, 22–26 May 2016.

composed of β-(1–4)-linked N-acetyl–D-glucosamine residues and is the main component of the exoskeleton of crustaceans, the fungal cell walls. CHT, obtained by alkaline deacetylation of chitin, is composed of randomly distributed β-(1–4)-linked D-glucosamine and N-acetyl-D-glucosamine [8,9]. CHT also shows excellent properties, such as low toxicity, low immunogenicity, superior biodegradability, biocompatibility [10]. In addition, CHT is an unmatched cationic polymer with gel-and film forming properties that readily forms polyelectrolyte complexes with negatively charged entities [11]. The chelating properties of CHT and derivatives can be attributed to the presence of a large number of functional groups (e.g., acetamido, primary amino, and/or hydroxyl groups) that are capable of coordinating with different contaminants [12].

After adsorption, it can be difficult or expensive to separate nanochitosan-based adsorbents from the aqueous solution using conventional separation techniques such as filtration and sedimentation. To overcome the problems related to the difficulty of separation and regeneration of nano-adsorbents, recent research has been focused on magnetic separation technology [13]. Magnetic nanoparticles, magnetite (Fe_3O_4), its oxidized form maghemite (γ-Fe_2O_3), have recently drawn considerable attention in potential applications such as magnetic separation, biosensors and drug delivery. Although Co (Co_3O_4, or $CoFe_2O_4$ form) and Ni are also highly magnetic materials, they are toxic and easily oxidized [5]. Magnetic nanoparticles with the aid of magnetic force can be separated from the water efficiently regardless of their nano-size [14]. As magnetite (Fe_3O_4) shows high dispersion stability, excellent biocompatibility, high magnetic susceptibility, and chemical stability, it has been widely used as magnetic material [15]. To synthesize magnetic nanoparticles, different methods such as microemulsion, precipitation, laser pyrolysis, sol-gel, thermal decomposition methods are used [16]. In chemical precipitation method, nanoparticles are generally obtained by addition of a base into aqueous solution of Fe(II) and Fe(III) salts [17–18]. The chemical reaction of Fe_3O_4 precipitation is given by the following equation [19,20],

$$2Fe^{3+} + Fe^{2+} + 8OH^- \leftrightarrow 2Fe(OH)_3\,(s) + Fe(OH)_2\,(s) \rightarrow Fe_3O_4\,(s) + 4H_2O$$

The CHT-coated MNPs are synthesized by coating method which is alkaline coprecipitation of Fe(II) and Fe(III) precursors in aqueous solutions of hydrophilic CHT polymers. The encapsulation of preformed iron oxide nanoparticles are stabilized by crosslinking CHT with tripolyphosphate (TPP) salts. The amino groups on the CHT particle become protonated in an acidic environment. With respect to mechanism proposed by Unsoy et al. [21], CHT is able to interact with negatively charged molecules, such as the hydroxyl (Fe-OH) groups on the surface of magnetite nanoparticles. The hydrophilic Fe_3O_4 cores precipitate by forming nuclei and rapidly adsorb well-dissolved CHT polymers [22]. When cationic CHT molecules are adsorbed onto the surface of anionic MNPs with electrostatic interactions, TPP, a polyvalent anion with three negatively charged phosphate groups, is added to the medium for ionic crosslinking of the CHT molecules with each other [23]. The addition of TPP cross-links the adsorbed CHT molecules to each other through the ionic interactions between the positively charged amino groups of CHT and negatively charged TPP [24]. To stabilize each distinct nanoparticle, uniform layers of CHT polymers were combined by physical cross-linking induced by electrostatic interaction on Fe_3O_4 cores [21,25–27].

Oladoja et al. synthesized a novel magnetic, macro-reticulated cross-linked chitosan (MRC) for the removal of tetracycline from water. Gastropod shells, a source of biogenic waste are used as the pore-forming agent, and magnetide as the magnetic-inducing particle. To decrease solubility of CHT in acidic media, CHT was modified by inserting crosslinks and glutaraldhyde was used as cross-linker. The interactions between tetracycline and the MRC surface was shown to occur via a monolayer sorption of tetracycline onto heterogeneous surfaces of varied affinities and chemisorption was reported to be the dominant mechanism of tetracycline sorption onto the MRC. The theoretical maximum monolayer sorption capacity of tetracycline on MRC was recorded to be 20.704 mg/g with respect to the Langmuir model [1]. To increase the mechanical properties of CHT, nanosized inorganic materials such as hydroxyapatite, nanoclay (halloysite nanotube, HLT), carbon nanotubes, titanium dioxide and graphene are incorporated into CHT [28]. Ma et al., prepared CHT/HLT-Fe_3O_4 microspheres by emulsion cross-linking method. The microspheres showed good adsorption capacity and regeneration property, no apparent deterioration at least three repeated cycles in efficiency and could be easily and rapidly separated from solution phase with the aid of magnetic force. The adsorption kinetics of the tetracycline on CHT/HLT-Fe_3O_4 was better described by the pseudo-second order equation and chemical process could be the rate-limiting step. It was also shown that the adsorption capacity of the CHT/HLT-Fe_3O_4 microspheres increased with the increasing concentration of tetracycline, and the maximum adsorption capacity was recorded to be 26.68 mg/g [2].

In this study, CHT-based nanoparticles loaded with iron oxide (Fe_3O_4) nanoparticles were gained magnetic properties. Then tetracycline antibiotic removal from medical wastewaters using CHT MNPs was investigated.

2. Materials and methods

2.1. Preparation of magnetic CHT nanoparticles

CHT coated magnetic iron oxide nanoparticles were synthesized by the precipitation of Fe(II) and Fe(III) salts in the presence of CHT and tripolyphosphate (TPP) molecules [21,29]. CHT was dissolved in 1% acetic acid, and the pH was adjusted to 4.8 by NaOH. Iron salts (1.34 g of $FeCl_2{\cdot}4H_2O$ and 3.40 g of $FeCl_3{\cdot}6H_2O$) were dissolved in 0.5% CHT solution. TPP and NH_4OH were added to the solution and the mixture was stirred vigorously at 2500 rpm. The colloidal CHT coated magnetic Fe_3O_4 nanoparticles were stirred for 1 h, then washed with deionized water and separated by magnetic decantation for several times.

2.2. Characterization of CHT MNPs

FTIR spectra of CHT, Fe_3O_4 nanoparticles and CHT MNPs were recorded on a Thermo Scientific Nicolet 6700 FTIR with 4 cm^{-1} resolution in the range of 4000–525 cm^{-1} using ATR. The obtained spectra was an average of 32 scans.

Samples of blank CHT, Fe_3O_4 nanoparticles and CHT MNPs were freeze-dried before undergoing thermogravimetric analysis. TGA and DSC analyses were carried out for powder samples under N_2 gas flow rate of 200 cm^3 min^{-1} using a SII EXSTAR 6000 TG/DTA 6300 TGA and Perkin Elmer Diamond DSC. In TGA, samples weighing 5 mg were heated from 30°C to 700°C at a heating rate of 10°C min^{-1} in N_2. In DSC, samples were heated from 0°C to 500°C.

The size distribution of the CHT MNPs was measured by a Malvern zetasizer model Nano ZS–90 (Malvern Instruments Ltd., UK). Dynamic light scattering was performed by the zetasizer to measure the size. The Z-average diameter of CHT MNPs was detected to be 803.7 nm. Synthesized CHT MNPs particles usually have broad and partially non-uniform size distribution.

2.3. Tetracycline adsorption experiments

The tetracycline adsorption experiments by CHT MNPs were performed on a temperature-controlled orbital incubator shaker set at 150 rpm maintained at 25°C for 48 h. The effects of the initial pH value of tetracycline solution, the amount of CHT MNPs, the initial concentration of tetracycline solution on the removal of tetracycline by CHT MNPs were investigated. The pH of the adsorption medium was initially adjusted the required value using either HCl or NaOH (1, 0.1 or 0.01 M solutions). The values of parameters which will be investigated the effect on adsorption, eg., pH was changed between 2.0–9.0, initial tetracycline concentration between 5–50 mg/L, amount of nanoparticle between 0.5–2.0 g/L. A certain amount of CHT MNPs was mixed with 100 mL of respective tetracycline solutions, whose concentration and initial pH were previously adjusted. Before mixing the CHT MNPs with the tetracycline-bearing solution, samples were taken from the sorption media. Subsequently, samples were taken at 2–5 min intervals at the beginning of sorption and at 15–30–60 min intervals before adsorption equilibrium was reached. After the tetracycline adsorption, the CHT MNPs were separated rapidly from the adsorption medium by magnetic decantation. The tetracycline adsorption efficiency was determined by measuring the amount of tetracycline remained in the supernatant with a UV spectrophotometer at 360 nm.

3. Results and discussion

In this study, the method of coprecipitation of iron salts in the presence of CHT and TPP was applied. The CHT MNPs were characterized by FTIR, TGA and DSC and then were used as adsorbents for the removal of tetracycline from aqueous solution. The effects of pH, adsorbent dosage, initial concentration of tetracycline and contact time on tetracycline adsorption on CHT MNPs were investigated. The adsorption kinetics and equilibrium of tetracycline on CHT MNPs were represented by pseudo-first and second-order equations and adsorption isotherms.

3.1. Fourier transform infrared spectroscopy (FTIR)

FTIR is extensively used analytical method for obtaining information about the availability of certain functional groups in the structure of the CHT MNPs and for measuring the binding mechanism of inorganic or organic contaminants. FTIR spectra of CHT included the following peaks : 3354 cm^{-1} for O–H bond stretching and N–H bond stretching, 2889 cm^{-1} for C–H, 1150 cm^{-1} for C–N strech and 1024 cm^{-1} for C–OH bond stretching. CHT MNPs showed the following peaks: ~3124 cm^{-1} due to amine N–H stretching vibration and –OH moieties in the chitosan, ~1594 cm^{-1} due to N–H scissoring from the primary amine because of free amino groups in the crosslinked chitosan, 1029 cm^{-1} for C–N, and ~585 cm^{-1} for the Fe–O group due to pure Fe_3O_4 (Fig. 1).

Fourier transform infrared spectroscopy (FTIR) is used to explain the chemical composition of synthesized nanoparticles. The presence of Fe_3O_4 core was specified by the strong stretching absorption band at 572 cm^{-1}, which corresponded to the Fe–O bond (MNP). In the CHT-coated nanoparticle's spectra, the peak observed in the 585 cm^{-1} region verified that the CHT nanoparticle contain magnetite (CHT MNP). In the IR spectrum of CHT, the band at 1589 cm^{-1} was detected to NH_2 group bend scissoring and the peak at 1375 cm^{-1} to OH bending of primary alcoholic group. In both CHT and CHT coated magnetic nanoparticle's spectra, the peaks around 1589 ± 5 cm^{-1}, identified the NH_2 group bend scissoring, were obtained. It was demonstrated that magnetite nanoparticles were successfully coated by CHT biopolymer. Briefly, in the spectrum of CHT MNP, the 1589 cm^{-1} peak of NH_2 group bend scissoring in CHT was shifted to 1594 cm^{-1}, and a new sharp peak at 585 cm^{-1} indicating the Fe–O bond was come in sight. All characteristic peaks of CHT and magnetite were observed in the spectrum of CHT MNP and these peaks were also verified with the related literatüre [16,21,25,27].

3.2. Thermal gravimetric analysis (TGA) and differential scanning calorimetry analysis (DSC)

Thermogravimetry has proven to be powerful analytical techniques that monitor the physical and chemical changes that take place during the heating of CHT MNPs and allow for a determination of chemical structure and

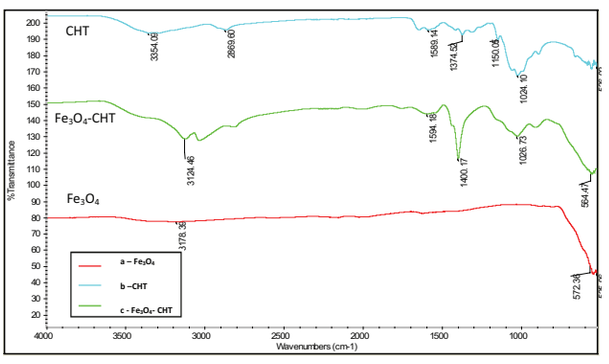

Fig. 1. FTIR spectra of (a) the naked Fe_3O_4, (b) CHT, and (c) Fe_3O_4-CHT nanoparticles.

composition. Thermal degradation studies are used for predicting the relative amounts of CHT and Fe_3O_4 in CHT MNPs. The qualitative and quantitative information about the volatile components of the magnetite and CHT MNPs were ensured via TGA analysis. The weight loss of uncovered MNPs over the temperature range from 30 to 800°C was about 1.9% (Fig. 2). This weight loss was due to the loss of residual water in the magnetite sample. For magnetic iron oxide nanoparticles, a significant, sharp peak was not observed in the DSC curve (Fig. 3). The CHT and CHT MNPs gave their specific TGA curves, which can ensure markers of the content of CHT biopolymers. The weight loss of Fe_3O_4 coated with CHT was small below 300°C because of the removal of absorbed physical and chemical water. When the temperature was raised to higher than 500°C, the weight loss was significant because CHT was degraded. Significant weight loss from 500°C to 700°C was not observed, implying the presence of only iron oxide within the temperature range. The amount of CHT bound on magnetite was calculated from the percentage weight loss in the TGA curve. The average mass content of CHT in MNPs by TGA was found to be about 36.2%. The thermochemical behavior defined by the TGA curve was consistent with that indicated by the DSC curve. However, the decomposition thermograms for CHT and CHT MNPs can vary between studies, recommending that the inlet of Fe_3O_4 nanoparticles into the complex reduces crystallization.

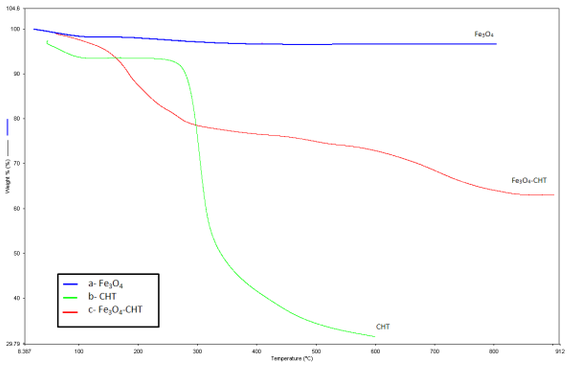

Fig. 2. Thermogravimetric analysis (TGA) of (a) the naked Fe_3O_4, (b) CHT, and (c) Fe_3O_4-CHT nanoparticles.

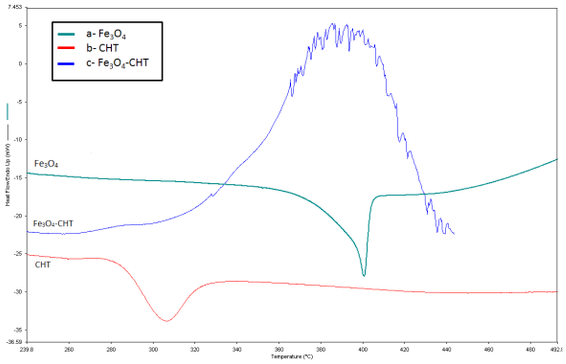

Fig. 3. Differential scanning calorimetry analysis (DSC) of (a) the naked Fe_3O_4, (b) CHT, and (c) Fe_3O_4-CHT nanoparticles.

3.3. Effect of pH on tetracycline adsorption on CHT MNPs

The variation in pH can not only affect the protonation-deprotonation transition of functional groups on CHT MNPs, but also can result in different charges on different sites of tetracyclines depending on solution pH. The pK_{a1}, pK_{a2}, pK_{a3} values of tetracycline are 3.30, 7.70, and 9.70, respectively. In this study, the effect of pH on the adsorption capacity of CHT MNPs was investigated at pH 3.0, 5.0, 7.0 and 8.5 depending on surface charge of magnetic nanoparticles and pK_a values of tetracycline. When solution pH is below 3.3, tetracycline exists in solution as a cation (TCH_3^+), due to the protonation of dimethyl-ammonium group. At pH between 3.3 and 7.7, tetracycline presents as a zwitterion (TCH_2^0), due to the loss of a proton from the phenolic diketone moiety. At solution pH greater than 7.7, tetracycline becomes as anion (TCH^- or TC^{2-}) due to the loss of protons from the tri-carbonyl system and phenolic diketone moiety. When pH of the tetracycline solution is between pK_{a1} and pK_{a2}, tetracycline is an amphoteric ion, nearly all of tetracycline molecules does not carry net electrical charge. On the other hand, the pK_a of CHT nanoparticles is around 6.20, below pH 5.0 almost 90% of active sites are protonated [4]. For that reason the adsorption capacity of CHT nanoparticles decreased when the solution pH decreased from 5.0 to 3.0. A bell-shaped pH dependence with highest equilibrium tetracycline adsorption capacity around pH 5.0 was observed (Fig. 4). As pH increases from 5.0 to 8.5, the dominant species of tetracycline changed from being neutral or zwitterionic to negatively charged. Electrostatic repulsion between similar charges of tetracycline and CHT MNPs was greater at either lower pH (positive-positive repulsion) or higher pH (negative-negative repulsion), thus creating a maximum electrostatic attraction at the intermediate pH range. The adsorption equilibrium between the amount of tetracycline adsorbed per unit weight of CHT MNPs and tetracycline unadsorbed concentration in solution was established at the end of 24 h, and the release of tetracycline from CHT MNPs was not observed during this time. The maximum amount of tetracycline adsorbed per unit weight of CHT MNPs and adsorption efficiency at pH 5.0, at 20 mg/L initial tetracycline concentration and at 0.5 g/L adsorbent dosage was found as 36.77 mg/g and 85.6%, respectively. The amount of tetracycline adsorbed per unit

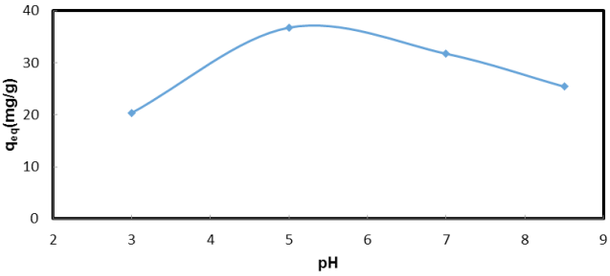

Fig. 4. Change of the amount of tetracycline adsorbed per unit weight of CHT MNPs at equilibrium with pH.

weight of CHT MNPs and adsorption efficiency at pH 3.0 decreased to 20.37 mg/g and 50.6%, respectively.

3.4. Effect of adsorbent dosage on tetracycline adsorption on CHT MNPs

When the dosage of CHT MNPs was increased from 0.5 g/L to 2.0 g/L, the amount of tetracycline adsorbed per unit weight of CHT MNPs decreased (Fig. 5). The decrease in q with increase in adsorbent dosage is due to complex interactions of several factors, there may be three main reasons. Firstly, this may be attributed to the tendency for CHT MNPs aggregates to form at higher adsorbent dosage, resulting in a decrease in active adsorption area. Secondly, the rate of adsorption is reduced at high sorbent concentrations, and hence more time is needed to reach equilibrium. Finally, the extent of desorption of adsorbed tetracycline from CHT MNPs will increase with increase in sorbent concentration, as a result of collision of sorbent nanoparticles, and the potential of multilayer adsorption will be reduced.

3.5. Effect of initial concentration of tetracycline and contact time on tetracycline adsorption on CHT MNPs

The effects of initial concentration of tetracycline and contact time on the adsorption capacity of tetracycline by CHT MNPs at 0.5 g/L adsorbent dosage and at pH 5.0 are shown in Fig. 6. The tetracycline adsorption capacity of CHT MNPs increased rapidly with the increasing contact time from 0 to 15 min. More than 80% of equilibrium tetracycline adsorption capacity of CHT MNPs was reached within 150 min. After 24 h, the tetracycline adsorption capacity of CHT MNPs remained constant and the adsorption equilibrium between the amount of tetracycline adsorbed per unit weight of CHT MNPs and tetracycline unadsorbed concentration in solution was established. Rapid increase in tetracycline adsorption capacity of CHT MNPs within 15 min can be ascribed to availability of more adsorption sites initially. After first 15 min, available adsorption sites of CHT MNPs were gradually filled by tetracycline molecules, then adsorption rate slowed down. To reach adsorption equilibrium absolutely, all adsorption experiments were carried out for 24 h.

When the initial concentration of tetracycline increased from 10 to 50 mg/L, the amount of tetracycline adsorbed per unit weight of CHT MNPs enhanced from 19.16 to 78.11 mg/g. This can be attributed to the fact that increases in the tetracycline concentration result in a large difference in concentration between CHT MNPs surface and tetracycline solution or a strong mass transfer driving force and further uptake of the tetracycline in the solution. The higher initial tetracycline concentration improves contact opportunity between CHT MNPs and tetracycline molecules, consequently adsorption rate and capacity rises. When the initial concentration of tetracycline was increased from 10 to 50 mg/L, the adsorption efficiency slightly decreased from 90.5 to 78.8 % at pH 5.0 (Fig. 7).

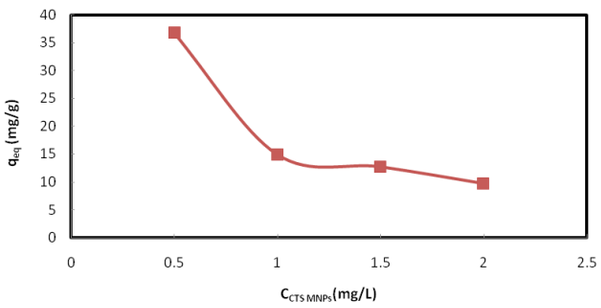

Fig. 5. Change of the amount of tetracycline adsorbed per unit weight of CHT MNPs at equilibrium with adsorbent dosage.

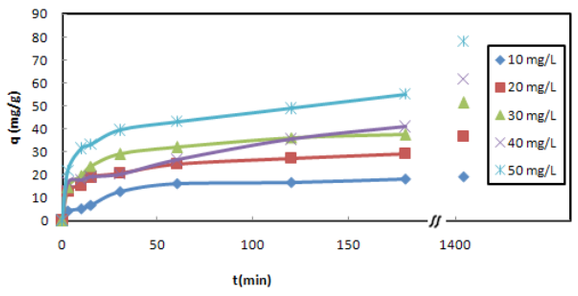

Fig. 6. Change of the amount of tetracycline adsorbed per unit weight of CHT MNPs with time and initial tetracycline concentration.

3.6. Adsorption isotherms of tetracycline adsorption on CHT MNPs

In order to optimize the design of an adsorption system to remove pollutants from wastewaters, it is important to define the most appropriate correlation for the equilibrium curve. The equilibrium adsorption isotherms are depicted by plotting the concentration of the tetracycline in the solid phase versus that in the liquid phase (Fig. 8). Comparing pH isotherms shows that well-adsorbed tetracycline has a increasing slope and was located in the upper surface concentration q_{eq} values, i.e. tetracycline adsorption at pH 5.0.

The adsorption equilibrium data were analyzed using the Langmuir and Freundlich models. The Langmuir model assumes that all sites are energetically equivalent [30].

$$q_{eq} = \frac{Q^o K C_{eq}}{1 + K C_{eq}} \quad (1)$$

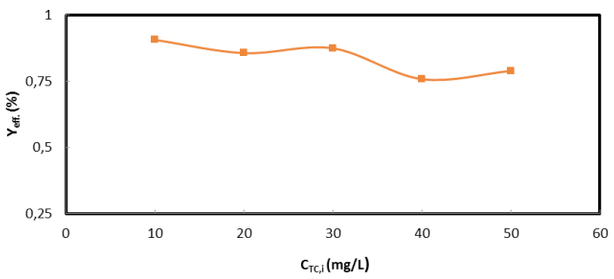

Fig. 7. Change of tetracycline adsorption efficiency with initial tetracycline concentration.

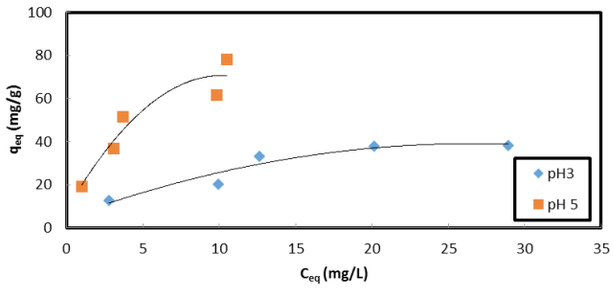

Fig. 8. Adsorption isotherms of tetracycline on CHT MNPs at different pH values.

where q_{eq} (mg/g) is the amount of adsorbate per unit weight of adsorbent in equilibrium with a solution concentration, C_{eq} (mg/L).

The Freundlich model assumes a logarithmic decrease in the heat of sorption with the fraction of surface covered by the sorbed solute [31]:

$$q_{eq} = K_F C_{eq}^{1/n} \quad (2)$$

The Freundlich isotherm model adequately fitted the equilibrium adsorption data of tetracycline on CHT MNPs both at pH 3.0 and 5.0, however, their adsorption isotherms were better fitted to the Langmuir equation (Fig. 9). This means that tetracycline adsorption on CHT MNPs occurs in accordance with the Langmuir assumptions. The tetracycline adsorption takes place at specific sites within the CHT MNPs. The CHT MNPs have a finite capacity for the tetracycline with monolayer adsorption. The tetracycline adsorption shows saturation kinetics, a saturation point at equilibrium is reached where no further adsorption can occur. The CHT MNPs are structurally homogeneous, so all sites are identical and energetically equivalent and a tetracycline molecule occupies a site and does not affect another tetracycline molecule trying to hold on to the surface. Relevant adsorption parameters were calculated according to both the Freundlich and Langmuir models at pH 3.0 and pH 5.0. The intercept of the Langmuir isotherm Q° is the amount of adsorbate per unit weight of adsorbent to form a complete monolayer on the surface (Table 1). Q° represents

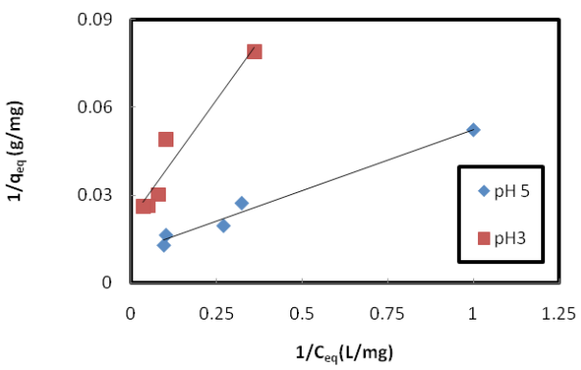

Fig. 9. Langmuir adsorption isotherms for the tetracycline adsorption on CHT MNPs at different pH values.

Table 1
Langmuir adsorption constants for the tetracycline adsorption on CHT MNPs at different pH values

pH	a ($L \cdot g^{-1}$)	b ($L \cdot mg^{-1}$)	q_s ($mg \cdot g^{-1}$)	R^2
3.0	6.146	0.135	45.662	0.912
5.0	23.868	0.253	94.340	0.980

the adsorption capacity when the surface of CHT MNPs is saturated with tetracycline. In other words, Q° is the maximum value of q_{eq}, tetracycline adsorption on CHT MNPs is by a monolayer type of adsorption in which the surfaces of nanoparticles are not saturated. The Langmuir constant K is a constant relate to the energy of adsorption. A large value of K also implies strong bonding. The larger the value of K, the greater is the fractional surface coverage at a fixed temperature and at a fixed value of C_{eq}. The highest Q° and K values were found to be 94.340 (mg/g) and 0.253 (L/mg) at pH 5.0.

The intercept K_F of the Freundlich isotherm is an indication of adsorption capacity of the adsorbent; the slope $1/n$ indicates the effect of concentration on the adsorption capacity and represents the adsorption intensity (Fig. 10). If adsorption is favorable, then $1/n < 1$ or $n > 1$. The closer the n value of the Freundlich adsorption equation is to zero, the more heterogeneous is the system (Table 2). The higher n values showed that the tetracycline adsorption on CHT MNPs approaches homogeneous system verifying the Langmuir assumptions. The highest K_F value was found to be 20.497 $mg^{(1-1/n)}\ g^{-1}\ L^{-n}$ at pH 5.0.

3.7. Kinetic models for tetracycline adsorption on CHT MNPs

The Lagergren–first–order rate equation is the most popular kinetics equation and generally expressed as follows [32]:

$$\frac{dq_t}{dt} = k_1(q_e - q_t) \quad (3)$$

After integration and applying boundary conditions, for $t = 0$, $q_t = 0$ and $t = t$, $q_t = q_t$, the integrated form of Eq. (3) becomes [33]

$$\log(q_e - q_t) = \log q_e - k_1 t \quad (4)$$

The adsorption rate constant k_1 can be determined experimentally by plotting log ($q_e - q_t$) vs. t (Fig. 11). The experimental kinetic data of tetracycline adsorption on CHT MNPs deviated considerably from the theoretical data of the pseudo-first order model. The parameter $q_{eq,theo.}$ values found from the intercept of a plot of log ($q_{eq} - q$) vs t also deviated substantially $q_{eq,exp}$ (Table 3). As chemisorption tends to become unmeasurably slow, the amount adsorbed is still significantly lower than the amount adsorbed at equilibrium. One suggestion for the differences in experimental and theoretical q_{eq} values is that there is a time lag, possibly due to a boundary layer or external mass transfer resistance controlling at the beginning of the adsorption [34]. The pseudo-first order adsorption rate expression of

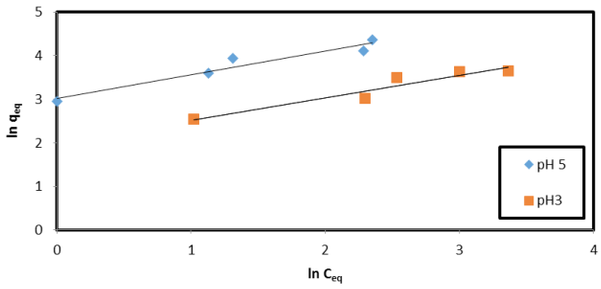

Fig. 10. Freundlich adsorption isotherms for the tetracycline adsorption on CHT MNPs at different pH values.

Table 2
Freundlich adsorption constants for the tetracycline adsorption on CHT MNPs at different pH values

PH	K_F ($mg^{(1-1/n)}$ g^{-1} L^{-n})	$1/n$	n	R^2
3.0	7.478	0.513	1.949	0.930
5.0	20.497	0.547	1.828	0.940

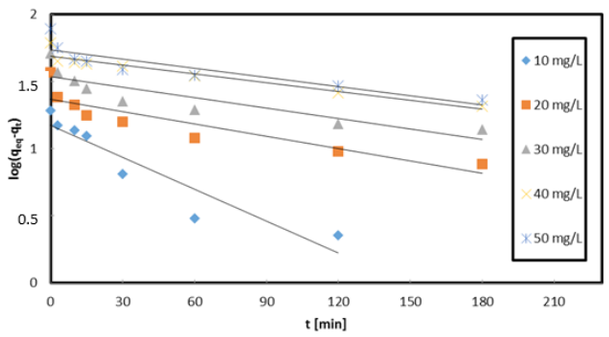

Fig. 11. Lagergren first order adsorption kinetics of tetracycline on CHT MNPs at various initial concentrations.

Table 3
Change of the Lagergren-first order rate constants with initial tetracycline concentrations

C_i (mg/L)	$q_{eq,exp.}$ (mg/g)	$q_{eq,theo.}$ (mg/g)	Error (%)	k_1 (1/min)	R^2
10	19.160	14.955	21.95	1.82×10^{-2}	0.881
20	36.766	23.367	36.44	7.14×10^{-3}	0.807
30	51.401	34.300	33.27	5.99×10^{-3}	0.765
40	61.483	48.809	20.61	5.07×10^{-3}	0.915
50	78.112	54.113	30.72	5.30×10^{-3}	0.790

Lagergren does not fit well the experimental data for the whole range of contact time and the plots are only linear at the beginning of adsorption (approximately the first 30 min). The Lagergren equation appeared to characterize the adsorption of tetracycline on CHT MNPs over 120–180 min.

If the rate of adsorption is a second order mechanism, the pseudo-second order desorption rate equation is given as [35]

$$\frac{dq_t}{dt} = k_2\left(q_e - q_t\right)^2 \tag{5}$$

After definite integration by applying the conditions $q_t = 0$ at $t = 0$ and $q_t = q_t$ at $t = t$, Eq. (5) becomes

$$\frac{t}{q_t} = \frac{1}{k_2 q_e^2} + \frac{t}{q_e} \tag{6}$$

The values of kinetic constants, k_2 and q_e, can be calculated from the plot of t/q_t against t (Fig. 12). The pseudo-second order kinetic model, in contrast to the pseudo-first order model, provided a good correlation for the tetracycline adsorption on CHT MNPs. As also seen from Table 4, the pseudo-second order rate constant value, k_2, was highly dependent on the initial tetracycline concentration. When the initial tetracycline concentrations are increased, the time necessary to attain an adsorption equilibrium prolongs. For that reason, k_2 is expected to decrease with the increasing initial drug dosage, the longer time is required [36]. The pseudo-second order kinetic model is based on the assumption that the rate limiting-step may be chemisorption. The second-order models generally used to define chemical and physical nonequilibrium are the two-site or bicontinuum models. These models suppose

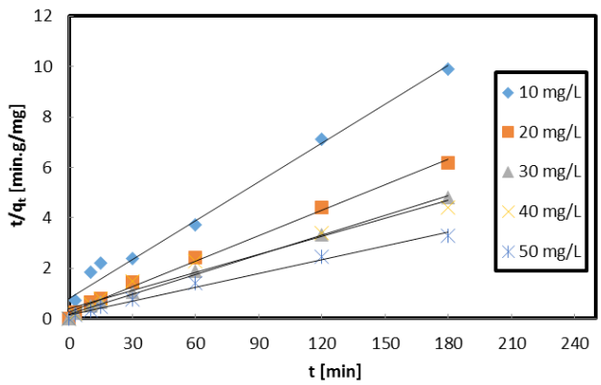

Fig. 12. Pseudo second order adsorption kinetics of tetracycline on CHT MNPs at various initial concentrations.

Table 4
Change of the pseudo-second order rate constants with initial tetracycline concentrations

C_i (mg/L)	k_2 (g/mg·min)	R^2
10	3.25×10^{-3}	0.982
20	4.61×10^{-3}	0.995
30	3.54×10^{-3}	0.996
40	1.52×10^{-3}	0.963
50	2.19×10^{-3}	0.990

that two reactions are occurring either in series or in parallel. First reaction is rapid, reaches equilibrium quickly, and generally called as physical adsorption. The second is a slower reaction that can continue for long time periods, and generally named as chemisorption. As q_{eq} and k_2 can be determined from the slope and intercept of the linear form of the pseudo-second order rate equation, contrary to the Lagergren rate expression there is no need to know any parameter beforehand.

4. Conclusion

A magnetically responsive iron oxide nanoparticle system coated by CHT nanoparticles was successfully developed for tetracycline removal from medical wastewaters. The binding of CHT to the MNPs was demonstrated by the measurement of FTIR, TGA and DSC. TGA results indicated that the CHT content of CHT MNPs was determined as 36.2% by weight. Maximum tetracycline adsorption capacity and efficiency by CHT MNPs was obtained at 50 mg/L initial tetracycline concentration, 0.5 g/L adsorbent dosage and at pH 5.0, and found to be 78.11 mg/g and 78.8%, respectively. The adsorption kinetics of tetracycline on CHT MNPs was better described by the pseudo-second-order rate expression, and their adsorption isotherms were better fitted to the Langmuir model. The CHT MNPs developed in this study had high tetracycline adsorption capacity and could be easily and rapidly separated from solution phase with the aid of magnetic force.

Acknowledgements

The authors wish to thank Middle East Technical University Central Laboratory for the size distribution measurements of the CHT MNPs by a Malvern Zetasizer Model Nano ZS–90.

References

[1] N.A. Oladoja, R.O.A. Adelagun, A.L. Ahmad, E.I. Unuabonah, H.A. Bello, Preparation of magnetic, macro-reticulated cross-linked chitosan for tetracycline removal from aquatic systems, Colloid Surface B, 117 (2014) 51–59.
[2] W. Ma, J. Dai, X. Dai, Z. Da, Y. Yan, Preparation and characterization of chitosan /halloysite magnetic microspheres and their application for removal of tetracycline from an aqueous solution, Desal. Water Treat., 57 (2016) 4162–4173.
[3] J. Dai, X. Wei, Z. Cao, Z. Zhou, P. Yu, J. Pan, T. Zou, C. Li, Y. Yan, Highly-controllable imprinted polymer nanoshell at the surface of magnetic halloysite nanotubes for selective recognition and rapid adsorption of tetracycline, RSC. Adv., 4 (2014) 7967–7978.
[4] L. Zhang, X. Song, X. Liu, L. Yang, F. Pan, J. Lv, Studies on the removal of tetracycline by multi-walled carbon nanotubes, Chem. Eng. J., 178 (2011) 26–33.
[5] J. Dai, Z. Zhou, C. Zhao, X. Wei, X. Dai, L. Gao, Z. Cao, Y. Yan, Versatile method to obtain homogeneous imprinted polymer thin film at surface of superparamagnetic nanoparticles for tetracycline binding, Ind. Eng. Chem. Res., 53 (2014) 7157–7166.
[6] W.-R. Chen, C.-H. Huang, Adsorption and transformation of tetracycline antibiotics with aluminum oxide, Chemosphere, 79 (2010) 779–785.
[7] G. Crini, Recent developments in polysaccharide-based materials used as adsorbents in wastewater treatment, Prog. Polym. Sci., 30 (2005) 38–70.
[8] F. Shahidi, R. Abuzaytoun, Chitin, chitosan, and co-products: chemistry, production, applications, and health effects, Adv. Food. Nutr. Res., 49 (2005) 93–135.
[9] M. Bodnar, J.F. Hartmann, J. Borbely, Preparation and characterization of chitosan-based nanoparticles, Biomacromolecules, 6 (2005) 2521–2527.
[10] M. Liu, Y. Zhang, C. Wu, S. Xiong, C. Zhou, Chitosan/halloysite nanotubes bionanocomposites: Structure, mechanical properties and biocompatibility, Int. J. Biol. Macromol., 51 (2012) 566–575.
[11] J. Synowiecki, N.A. Al-Khateeb, Production, properties, and some new applications of chitin and its derivatives, Crit. Rev. Food. Sci., 43 (2003) 145–171.
[12] A. Rampinoa, M. Borgognaa, P. Blasi, B. Bellich, A. Cesàro, Chitosan nanoparticles: Preparation, size evolution and stability, Int. J. Pharm., 455 (2013) 219– 228.
[13] M. Faraji, Y. Yamini, M. Rezaee, Magnetic nanoparticles: Synthesis, stabilization, functionalization, characterization, and applications, J. Iran. Chem. Soc., 7 (2010) 1–37.
[14] J. Gómez-Pastora, E. Bringas, I. Ortiz, Recent progress and future challenges on the use of high performance magnetic nano-adsorbents in environmental applications, Chem. Eng. J., 256 (2014) 187–204.
[15] A.-H. Lu, E.L. Salabas, F. Schüth, Magnetic nanoparticles: Synthesis, protection, functionalization, and application, Angew. Chem. Int. Ed., 46 (2007) 1222–1244.
[16] R.G. López, M.G. Pineda, G. Hurtado, R.D. de León, S. Fernández, H. Saade, D. Bueno, Chitosan-coated magnetic nanoparticles prepared in one step by reverse microemulsion precipitation, Int. J. Mol. Sci., 14 (2013) 19636–19650.
[17] L. Xu, , M.-J. Kim, K.-D. Kim, , Y.-H. Choa, H.-T. Kim, Surface modified Fe_3O_4 nanoparticles as a protein delivery vehicle, Colloid Surface A., 350 (2009) 8–12.
[18] W. Zhang, H. Shen, M.Q. Xie, L. Zhuang, Y.Y. Deng, S.L. Hu, Y.Y. Lim, Synthesis of carboxymethyl-chitosan-bound magnetic nanoparticles by the spraying co-precipitation method, Scripta Mater., 59 (2008) 211–221.
[19] M.C. Mascolo, Y. Pei, T.A. Ring, Room temperature co-precipitation synthesis of magnetite nanoparticles in a large pH window with different bases, Materials, 6 (2013) 5549–5567.
[20] T.K. Indira, P.K. Lakshmi, Magnetic nanoparticles – A review, Int. J. Pharm. Sci. Nanotechnol., 3 (2010) 1035–1042.
[21] G. Unsoy, S. Yalcin, R. Khodadust, G. Gunduz, U. Gunduz, Synthesis optimization and characterization of chitosan-coated iron oxide nanoparticles produced for biomedical applications, J. Nanopart. Res., 14 (2012) 964–977.
[22] P. Calvo, C. Remun˜an-Lo´pez, J.L. Vila-Jato, M.J. Alonso, Chitosan and chitosan/ethylene oxide-propylene oxide block copolymer nanoparticles as novel carriers for proteins and vaccines. Pharm. Res., 14 (1997) 1431–1436.
[23] S. Rodrigues, A.M.R. Costa, A. Grenha, Chitosan/carrageenan nanoparticles: Effect of cross-linking with tripolyphosphate and charge ratios, Carbohydr. Polym., 89 (2012) 282–289.
[24] S.T. Lee, F.L. Mi, Y.J. Shen, S.S. Shyu, Equilibrium and kinetic studies of copper(II) ion uptake by chitosan-tipolyphosphate chelating resin, Polym., 42 (2001) 1879–1892.
[25] D.H.K. Reddy, S.-M. Lee, Application of magnetic chitosan composites for the removal of toxic metal and dyes from aqueous solutions, Adv. Colloid Interface Sci., 201–202 (2013) 68–93.
[26] M. Khajeh, S. Laurent, K. Dastafkan, Nanoadsorbents: classification, preparation, and applications (with emphasis on aqueous media), Chem. Rev., 113 (2013) 7728–7768.
[27] G.-y. Li, Y.-r. Jiang, K.-l. Huang, P. Ding, J. Chen, Preparation and properties of magnetic Fe_3O_4-chitosan nanoparticles, J. Alloys Compd., 466 (2008) 451–456.
[28] W.S.W. Ngah, L.C. Teong, M. Hanafiah, Adsorption of dyes and heavy metal ions by chitosan composites: A review, Carbohydr. Polym., 83 (2011) 1446–1456.

[29] D. Kavaz, S. Odabaş, E. Güven, M. Demirbilek, E.B. Denkbaş, Bleomycin loaded magnetic chitosan nanoparticles as multi-functional nanocarriers, J. Bioact. Compat. Polym., 25 (2010) 305–318.
[30] L. Langmuir, The constitution and fundamental properties of solids and liquids, J. Am. Chem. Soc., 38 (1916) 2221–2295.
[31] H. Freundlich, Ueber die adsorption in Loesungen, Zeitschrift fuer Physikalische, Chemie, 57A (1907) 385–470.
[32] S. Lagergren, Zur theorie der sogenannten adsorption gelaster stoffe, Kungliga Svenska Vetenskapsakademiens, Handlingar, 24 (1898) 1–39.
[33] S. Azizian, Kinetic models of sorption: A theoretical analysis, J. Colloid Interf. Sci., 276 (2004) 47–52.
[34] N.A. Oladoja, I.A. Ololade, O.A. Alimi, T.A. Akinnifesi, G.A. Olaremu, Iron incorporated rice husk silica as a sorbent for hexavalent chromium attenuation in aqueous system, Chem. Eng. Res. Des., 91 (2013) 2691–2702.
[35] Y.S. Ho, G. McKay, Pseudo-second order model for sorption processes, Process Biochem., 34 (1999) 451–465.
[36] N.A. Oladoja, A. Ahmad, A.O. Adesina, Biogenic derived binary metal oxide as a reactive material for remediation of pyrophosphate contaminated aqua system, J. Water Process Eng., 3 (2014) 82–89.